Effects of the number of genome segments on primary and systemic infection for a multipartite plant RNA virus

Jesús A. Sánchez-Navarro[1a], Mark P. Zwart[1a#] and Santiago F. Elena[1,2]

[1]Instituto de Biología Molecular y Celular de Plantas, Consejo Superior de Investigaciones Científicas-UPV, València, Spain
[2] The Santa Fe Institute, Santa Fe, NM 87501, USA

[a] These authors contributed equally
[#] Corresponding author:
Instituto de Biología Molecular y Celular de Plantas, Consejo Superior de Investigaciones Científicas-UPV, CL Ingeniero Fausto Elio s/n, 46022 València, Spain
Tel: 34 963 877009 ext. 78368
Fax: 34 963 877859
E-mail: marzwa@upvnet.upv.es

Running title: Dose response of multipartite viruses

Abstract: 233 words

Manuscript main body: 6171 words

Display items: 5 Figures and 2 Tables

Multipartite plant viruses were discovered because of discrepancies between the observed dose response and predictions of the independent action hypothesis (IAH) model. Theory suggests that the number of genome segments predicts the shape of the dose response, but a rigorous test of this hypothesis has not been reported. Here *Alfalfa mosaic virus* (AMV), a tripartite *Alfamovirus*, and transgenic *Nicotiana tabacum* plants expressing none (wild-type), one (P2) or two (P12) viral genome segments were used to test whether the number of genome segments necessary for infection predicts dose response. Dose response for wild-type plants was steep and congruent with predicted kinetics for a multipartite virus, confirming previous results. Moreover, for P12 plants the data support the IAH model, showing that the expression of virus genome segments by the host plant can modulate the infection kinetics of a tripartite virus to those of a monopartite virus. However, the different types of virus particles occurred at different frequencies, with a ratio 116:45:1 (RNA1:RNA2:RNA3), which will affect infection kinetics and required analysis with a more comprehensive infection model. This analysis showed that each type of virus particle has a different probability of invading the host plant, both at the primary- and systemic-infection levels. Whilst the number of genome segments affects dose response, taking into consideration differences in the infection kinetics of the three types of AMV virus particles results in a better understanding of the infection process.

Introduction

There is great variation in the architecture of the genome between viruses; the nucleic acid used, its polarity in the case of RNA viruses, replication and transcription strategies, and genome size all vary between viruses. Moreover, this variation has important implications for virus biology and evolution, imposing limitations and providing opportunities. Another characteristic that varies between viral genomes is the number of genome segments, which are essentially analogous to chromosomes as they are the highest level of physical organization of the genome. Whereas many viral genomes are composed of only a single segment, some viruses have evolved genomes with multiple segments. For example, the *Orthomyxoviridae* have evolved six to eight genome segments, and reassortment of these segments during mixed-genotype infections is a key feature of their epidemiology and evolution (1, 2). Whereas for the *Orthomyxoviridae* all genome segments are packaged into a single virus particle, some plant viruses are multipartite: each segment is packaged individually into a virus particle (3). The number of genome segments for multipartite plant RNA viruses ranges from two (i.e., *Bymovirus*) to four (i.e., *Hordeivirus*), whereas the *Nanovirus* have single stranded DNA genomes comprised of six to eight ssDNA genome segments (4).

The existence of multipartite viruses was first suggested by observations that were at odds with predictions of the independent action hypothesis (IAH) model (5). The IAH model assumes that each virus particle has a non-zero probability of infection and that particles do not affect each other during the infection process (6-8). Many IAH model predictions have been confirmed experimentally for monopartite plant viruses (6, 7, 9-11). Given that different types of virus particles obligatorily need to complement each other for multipartite viruses, one would not expect the IAH model to hold for a multipartite virus. Multipartite viruses were indeed discovered due to the effects of multipartition on the relationship between dose and local-lesion number. Price and Spencer (12) first reported that the relationship between dose

47 and the number of local lesions for *Alfalfa mosaic virus* (AMV), *Tobacco necrosis virus* (TNV)
48 and *Tobacco ringspot virus* (TRSV) on local lesion hosts was steeper than predicted by the
49 IAH model. It was quickly recognized that these steep dose local-lesion relationships could
50 be explained if there were complementation between different types of virus particles (13,
51 14). The groundbreaking work of Fulton (5) finally put this hypothesis on firm ground.
52 Through a series of elegant experiments with *Sour cherry necrotic ringspot virus* (nowadays
53 renamed as *Prunus necrotic ringspot virus,* [PNRSV]) and *Prune dwarf virus* (PDV), Fulton
54 demonstrated that the dose local-lesion relationship was steeper than IAH predictions, and
55 that infectivity of the virus sometimes could be influenced by inactivated virus, depending on
56 whether the inactivation method degraded the viral RNA. The conclusion that at least two
57 particles were needed to cause infection was then confirmed by the discovery that
58 preparations of some plant viruses were comprised of two or more virus particles (3).
59 Moreover, preparations of a single type of particle had low infectivity, which was restored in
60 mixtures of the different types of particles.

61 Although there is strong experimental evidence that multipartition of the genome
62 affects infection kinetics (3, 5), numerous key issues related to the infection process of
63 multipartite viruses have not been addressed. First, all work on infection kinetics concerns
64 local lesions, meaning that the results cannot necessarily be extrapolated to infection of
65 permissive hosts. Moreover, the effects of multipartition on systemic infection have not been
66 considered. As it is precisely productive systemic infections that will result in between-host
67 transmission, this omission is biologically relevant. Will the kinetics of primary and systemic
68 infection in a permissive host conform to predictions for a multipartite virus? Second, if the
69 different particle types are not present at the same frequency, this may have a profound
70 effect on dose response. Consider the hypothetical example of a bipartite virus for which
71 one segment is one hundred times as abundant as the other, whilst both segments have the
72 same probability of entering host cells. In this case, the dose response will be limited and
73 shaped by the low frequency variant, because any site invaded by the low frequency variant

has probably already been invaded by the high frequency variant. Therefore, it needs to be considered if different particle types are present at the same frequency, and if they are not, what the ramifications are for infection kinetics. Finally, there are methodological limitations in the original pioneering study of Fulton (5): the comparison between data and models is not rigorous, and the testing of hypotheses is purely qualitative. Although Fulton´s work is seminal from a historical perspective, these shortcomings have not been addressed in subsequent studies to date.

Here the kinetics of multipartite virus infection was re-examined, using the tripartite AMV and *Nicotiana tabacum* plants as a model system. A study design that allows for a rigorous, quantitative analysis of whether the genome segment number predicts multipartite virus dose response and accounts for deviations from IAH model predictions was used. Three plants were used for dose-response experiments: *Nicotiana tabacum* L. cv. *Samsun* (henceforth referred to as ´wild-type plants´), a transgenic plant derived from *N. tabacum* cv. *Samsun* that expresses AMV genomic segment RNA2 under the *Cauliflower mosaic virus* 35S promoter (´P2 plants´), and a transgenic plant expressing AMV genomic segments RNA1 and RNA2 (´P12 plants) (15). Note that uncoated AMV RNA segments can achieve cell-to-cell movement (16-18), whereas for systemic movement the formation of virus particles, each again encapsidating a single RNA segment, is required (17). It has already been shown that the P2 and P12 transgenic plants can support full-blown AMV systemic infection in the absence of the expressed segment in the inoculum (15), and it was anticipated that the expressed RNA segments could therefore complement virus particles to generate primary or systemic infection. Here it was attempted to alter the infection kinetics of AMV from those of a tripartite virus to those of a bipartite or monopartite virus, by inoculating AMV into transgenic plants expressing one or two viral genome segments. These results show that the underlying mechanisms are more complex than previously thought and suggest reasons why multipartition might have evolved.

Materials and Methods

Preparation of viral stocks

Virus purification was performed from infected *Nicotiana benthamiana* plants inoculated with transcripts of RNAs 1, 2 and 3 obtained from an infectious clone of the AMV strain 425 Leiden. Virus particles were isolated 4 days post inoculation (dpi) as previously described (19). The purified particles were resuspended in PE buffer (10 mM NaH_2PO_4, 1 mM EDTA, pH 7.0), aliquoted in stocks of 50 µl and stored at -80 ºC until use.

Dose response experiments

Plants were kept in a growth chamber at 24 °C and 16 hours light for one week until transplantation from agar plates to soil. Thereafter they were kept in a greenhouse at 24 °C and 16 hours light. We opted for a large single-block experiment, given that any block-level experimental variation would tend to lead to smoother dose responses (20, 21). Fifteen 5-week-old plants were inoculated for each of eight virus doses obtained from a 5-fold dilution series in PE buffer, and as mock-infected controls. Each plant was rub-inoculated with 5 µl of serially diluted viral stock or only buffer, and Carborundum was used as an abrasive. Plants were monitored for the AMV-symptoms daily until 14 dpi.

Detection of AMV infection

The presence of AMV in inoculated and upper leaves was performed by tissue printing analysis using transversal section of the corresponding petiole, as described previously (22). The inoculated leaves were also analyzed by grinding the full leave with 10 volumes of cold extraction buffer (50 mM sodium citrate, 5 mM EDTA, pH 8.5), which was then directly applied to the membrane as described previously (23). RNA was fixed to the membrane with a UV cross-linker (700x100 µJ/cm^2). Hybridization and detection were conducted as

previously described (24) using a DIG-riboprobe (Roche Diagnostic GmbH) complementary to nt 1 - 964 (GenBank L00162.1) of AMV RNA4.

Quantification of viral stocks

Total RNA was extracted from purified virus particles using TRI REAGENT™ (Sigma-Aldrich, Inc.) and following the manufacturer's recommendations. Purified RNA was serially diluted (5-fold dilutions) in TE buffer and 1 µl of each dilution was directly applied on a nylon membrane together with serial dilutions of known amounts of *in vitro* transcribed RNAs 1, 2 and 3 of AMV. The quantification of the transcribed AMV RNAs was performed by spectrophotometer ND-1000 (Nanodrop®) and by agarose gel using a RNA ladder (RiboRuler High Range RNA Ladder 200 to 6000, Thermo Scientific). Replicas of the same membrane were hybridized with specific DIG-riboprobes for the AMV RNAs 1 (complementary to nt 350 - 861; GenBank L00163.1), 2 (complementary to nt 162 - 680; GenBank X01572.1), RNA3 (complementary to nt 369 - 1248; GenBank K03542.1), or the RNA4 (complementary to nt 1 - 964; GenBank L00162.1). Hybridization and detection was conducted as previously described (24) using a chemiluminiscent substrate and the LAS-3000 digital imaging system (FujiFilm). As AMV RNA4 is a subgenomic RNA of RNA3, the concentration of RNA4 was estimated by subtracting the estimated RNA3 concentration.

To estimate the number of genome equivalents present and their estimated frequencies, all data for the standard curve (input and readout values of known dilutions) were first $\log_{10}$-transformed to ascertain over what range the response was linear. The dynamic range was limited to one dilution before the response appears to saturate. Linear regression on the $\log_{10}$-transformed data was then performed, rendering high values for the coefficient of determination (mean r^2 ±SD = 0.994 ±0.006). For those samples that fell within the dynamic range, the estimated linear regression parameters were used to estimate the unknown concentrations in the virus samples. Finally the number of genome equivalents was calculated based on the length of the genome segment.

Estimating the area of primary infection foci in different plant types

N. tabacum plants wild-type, P1, P2 or P12 were inoculated with a mixture of capped transcripts corresponding to AMV RNAs 1, 2, a modified RNA3, which expresses the green fluorescent protein (GFP) (25) and a few micrograms of purified AMV CP as described in (26). The fluorescence derived from the chimeric AMV RNA3 encoding GFP was monitored using a Leica Stereoscopic Microscope. The area of infection foci was measured at 2 and 3 dpi, using ImageJ software (27).

A generalized linear model (GLM) was used to statistically analyze the data (SPSS 20.0), with the Akaike Information Criterion (AIC) used to establish that the best-supported model, using a gamma distribution and log link. Pairwise comparisons were made using the estimated marginal means with a Holm-Bonferroni correction. To test if there was an effect of type of plant on the proportion of systemically infected leaves, the lowest dose at which the majority of plants was infected for each plant genotype (1/625 dilution for wild-type, 1/3125 dilution for P2 and 1/78125 dilution for P12) was considered. The highest infected leaf was considered the limit of systemic infection, and the number of systemic leaves below the highest infected leaf positive for AMV infection was counted. A test of equal proportions was then performed (R 2.14), grouping the data by plant type. Pooled data of each plant type were used to perform pairwise comparisons, with a Holm-Bonferroni correction for multiple comparisons.

Modeling dose response: classic framework with equal frequencies of all types of virus particles

A simple framework for considering the dose response of a multipartite virus, which assumes that the different types of virus particles are present at the same frequency, is first described. This model is equivalent to the description given by Fulton (5), although little detail is given in that publication. However, here the model is geared to describing the frequency of primary

and systemic infection, rather than the number of local lesions.

It is assumed that each virus particle type acts independently in the infection process up to the point that it has successfully breached an epidermal cell and can then begin to support replication in the presence of the other necessary particle types, a part of the infection process that is subsequently referred to as ´invading´ the host plant. The different particle types will behave differently in this process (e.g., in the presence of RNAs 1 and 2, there will be replication of these segments (28)), but the complete cellular infection cycle cannot be completed unless all three particles have invaded a cell (15). The assumption of independence is warranted if the virus is only passively carried up until entering the cell, and if particles do not aggregate. The mean number of particles invading each cell is $\alpha_j d_j$, where α_j is the probability of that particle type j invading a cell and d_j is the dose of that particle type. Note that α needs to be carefully interpreted here, being a probability that reflects the ability of a segment to support virus replication. The assumption is then made that the number of particles of type j per cell, v_j, follows a Poisson distribution, such that $\Pr(v_j) = (\alpha_j d_j)^{v_j} e^{-\alpha_j d_j} / v_j!$, where j can take the values 1, 2, …, k (k = 3 for AMV). Therefore, the frequency at which a cell is infected by at least one particle of type j, C_j, will then be $C_j = 1 - \Pr(v_j = 0) = 1 - e^{-\alpha_j d_j}$. However, the virus can only replicate if all the necessary k particle types have invaded the cell. If the frequency of the particles in the inoculum is the same, then for each dose (a dilution of the inoculum) the dose of each particle type (d) in the inoculum will also be the same. If it is also assumed the probabilities of infection for each particle type are the same (e.g., $\alpha \equiv \alpha_1 = \alpha_2 = \ldots = \alpha_k$), and that the successful infection of one cell will eventually lead to observable infection of the inoculated leaf, then the frequency of infection in the inoculated leaf (I) will then be

(1) $$I = \prod_{j=1}^{k} C_j = \left(1 - e^{-\alpha d}\right)^k.$$

For systemic infection of a plant, there is an additional infection step that each particle type surmounts with a probability β_j. Moreover, it is assumed that there is heterogeneity in host plants in their susceptibility to systemic infection by the virus. This assumption is made because even at high doses not all plants are always infected. These cases would be extremely unlikely under a maximum-likelihood framework that did not include heterogeneity in host susceptibility, and hence would strongly affect model parameter estimates. Although heterogeneity in susceptibility could be modeled in detail (21), a simpler but in this case equally effective manner to take differences in susceptibility into account is to assume that only a fraction ψ of host plants can be systemically infected. If it is again assumed that systemic infection probabilities are the same for all particle types ($\beta \equiv \beta_1 = \beta_2 = \ldots = \beta_k$), the frequency of systemic infection in plants (I_s) will be

$$I_s = \psi\left(1 - e^{-\alpha\beta d}\right)^k. \quad (2)$$

For both equations 1 and 2, when $k = 1$ the model collapses to an IAH model that assumes that each particle and particle type act independently. Therefore, when $k = 1$, this model is referred to as the IAH model. When $k > 1$, the infection presented above is referred to as the dependent action (DA) model. Note that k can take values of less than 1, but this outcome is not expected here given previous results (5, 12). Note that for fitting the classic infection model, the combined dose (d) of all three particle types was used.

Modeling dose response: a general framework

A limitation of the classic framework for analysis of dose-response of multipartite viruses is that it does not take into account the possibility that the frequency of different particle types varies in the inoculum. Moreover, the probabilities of primary and systemic infection in the inoculated and systemic leaves may also not be the same for each particle type. A simple

model taking these three aspects into account is therefore introduced. For primary and systemic infection the probabilities that a plant will be infected are, respectively,

(3) $I = \prod_{j=1}^{k}\left(1 - e^{-\alpha_j d_j}\right)^{\omega}$ and

(4) $I_s = \psi \prod_{j=1}^{k}\left(1 - e^{-\alpha_j \beta_j d_j}\right)^{\omega}$,

where ω is introduced so that the interactions between particles of one particle type can be non-additive. When $\omega < 1$ there are antagonistic interactions between particles of one particle type, whereas when $\omega > 1$ there are synergistic interactions. When $\omega \neq 1$, the general model predictions are equivalent to those resulting from the classic model having an estimated k different from the actual number of genome segments. For dose response in transgenic plants expressing one or two viral RNA segments, the term for infection of these segments becomes 1 (i.e., all plants have undergone the equivalent of being invaded by expressing the RNA segments) and it is dropped from the model. I.e., for primary infection of P2 plants, which express AMV RNA2, the frequency of primary infection is $I = \left(1 - e^{-\alpha_1 d_1}\right)^{\omega}\left(1 - e^{-\alpha_3 d_3}\right)^{\omega}$ whereas for P12 plants it is $I = \left(1 - e^{-\alpha_3 d_3}\right)^{\omega}$.

To test whether the data support inclusion of model parameters, model selection was performed over a series of models based on equations 3 and 4. Model 1 assumes additive interactions between particle types ($\omega = 1$) and equal probabilities of primary and systemic infection between particle types ($\alpha \equiv \alpha_1 = \alpha_2 = \alpha_3$ and $\beta \equiv \beta_1 = \beta_2 = \beta_3$). Note that this model is only equivalent to the classic model if the frequency of different particle types is equal. Three parameters must therefore be estimated: α, β and ψ. Model 2 assumes no additive interactions between particles, but allows probabilities of infection for the different particle types to vary. The frequency of the different particle types was measured empirically, meaning that seven parameters must therefore be estimated: α_1, α_2, α_3, β_1, β_2, β_3, and ψ.

Model 3 allows for non-additive interactions between particles, but assumes that probabilities of infection are equal. Four parameters must therefore be estimated: α, β, ψ, and ω. Model 4 allows for non-additive interactions and allows probabilities of infection to vary for the different particle types. Eight parameters must therefore be estimated: α_1, α_2, α_3, β_1, β_2, β_3, ψ, and ω. Finally, Model 5 allows the probabilities of primary infection for the first and third particle types (α_1 and α_3) to be host-plant dependent and allows for non-additive interactions. (The second particle type is needed only for infection of the wild-type plant, and only a single estimate of α_2 is therefore needed.) Model 5 is therefore the least restricted model. Although it is probably over-parameterized, this model serves to test whether model fit can be further improved. Eleven parameters must be estimated: $\alpha_{1,WT}$, $\alpha_{1,P2}$, α_2, $\alpha_{3,WT}$, $\alpha_{3,P2}$, $\alpha_{3,P12}$, β_1, β_2, β_3, ψ, and ω.

Model fitting and selection

To fit the model to the data, a maximum likelihood approach was used. Given that each plant represents an independent observation, the likelihood of a model prediction for I_i is $L(I_i|X,Y) = \binom{X}{Y} {I_i}^Y (1-I_i)^{X-Y}$, where X is the total number of plants inoculated, and Y is the number of plants infected in the inoculated leaf, and likewise for systemic infection. From a biological perspective, a plant can only become systemically infected after successful primary infection has occurred. However, since primary and systemic infections were determined independently, the likelihood of systemic infection is also calculated over all the data and not just over the fraction of plants found to have primary infections. The model was fitted to the data for each plant type by first performing grid searches over large parameter spaces to ensure a global solution was found. Next, stochastic hill climbing was performed to determine exact parameter estimates. These searches were also performed on 1000 bootstraps of the data, to estimate the 95% confidence interval (CI) of the parameter estimates. AIC was then used to perform model selection.

The data used for modeling dose response have been deposited at Dryad: doi:NN.NNNN/dryad.XXXXX.

Results

Predictions of a simple infection model

The IAH model (equation 1) predicts a dose response with a singular shape (19), which can shift position depending on the infection probability (Fig. 1a). The same model can be extended to a multipartite virus, when it is assumed that (i) particles of each type act independently in invading the host (entering host cells, see Materials and Methods), and (ii) that particles of *k* types are necessary for infection, which corresponds to actual number of different segments. This infection model predicts a steeper dose response for multipartite viruses, if the frequency of particles and their probabilities of invading the host are the same (Fig. 1b-c). In this case, the number of genome segments determines the shape of the dose response, but it can again shift positions, depending on the infection probabilities of the different particle types (Fig.1b-c). However, if the frequency of different particle types is not the same or their infection probabilities are different, the dose response will tend to be shallower (Fig. 1d), approaching the IAH response when, for example, one of the genome segments is very rare (Fig. 1e). On the other hand, a steep dose response equivalent to simple model predictions for a tripartite virus can be achieved when the frequency of particles is not equal (Fig. 1f), but the product of dose and infection probability ($\alpha_j d_j$,) is approximately equal for all particle types.

One can therefore expect a steep dose-response for a multipartite virus corresponding to simple model predictions only under specific conditions. When these conditions are not met, the dose response will tend to be smoother. Moreover, any

311 experimental error (e.g., variation in virus dose or inoculum size) will also tend to make the
312 dose response smoother (20, 21). Therefore, the observation of steep responses for plant
313 multipartite viruses seems to be somewhat unlikely from the outset, and its apparent
314 commonality is therefore striking (5, 12).
315
316 **Rejection of IAH model for AMV infection of wild-type and P2 plants**
317 Recent work on IAH for *Tobacco etch virus* (TEV), a monopartite *Potyvirus*, confirmed
318 various IAH model predictions (7, 10, 11). On the other hand, the relationship between AMV
319 dose and the number of local lesions has been reported to be steeper than IAH predictions
320 (12). Therefore, we first set out to confirm that the data for the infection of wild-type and P2
321 plants do not support the IAH model, whereas data for the P12 plants were expected *a priori*
322 to support the IAH model. This analysis with the classic infection model was performed to
323 test whether these experimental results and analysis are compatible with historical results.
324 Equations 1 and 2 were fitted to the data, with a separate analysis for wild-type, P2 and P12
325 plants (see Materials and Methods). For wild-type plants, it was indeed found that the DA
326 model was better supported than the IAH model (Table 1), as the dose response was
327 steeper than IAH model predictions (Fig. 2a). For P2 plants the DA model was also better
328 supported than the IAH model (Table 1), as the dose response for P2 plants was also
329 steeper than IAH predictions (Fig. 2b). The steep dose response for both wild-type and P2
330 plants is also shown by k values significantly greater than 1 (Table 1). On the other hand, for
331 P12 plants, IAH was the best-supported model (Table 1) and dose response was very similar
332 to model predictions, being shallower then for P2 or wild-type plants (Fig. 2c).
333
334 **Frequency of AMV particle types**
335 The frequency of the three different AMV particle types was then considered, because these
336 frequencies should be equal in order for an analysis with the classical model to be pertinent.
337 However, it was found that particle types were present at different frequencies in the virus

stock. The observed ratio (± SD) RNA1:RNA2:RNA3:RNA4 was 116.4 ±17.5 : 44.8 ±8.0 : 1.0 ±0.3 : 123.6 ±23.7, meaning that RNA3 is relatively scarce. Note that RNA4 was included in this analysis, but is not required for infection (15).

General infection model suggests particle-dependent probability of invading the host

Initial analysis of the data using the classic infection model suggests the DA model is supported for AMV infection of wild-type and P2 plants, whereas the IAH model is supported for infection of P12 plants. However, given that there are differences in the frequency of the different particle types, the data were analyzed with a general infection model (see Materials and Methods). This second analysis was performed for the data of all three plants types at once. Moreover, this approach has the added benefit that it allows testing not only whether the different particle types have different invasion probabilities, but also whether these invasion probabilities are independent of the presence of other particle types (i.e., host-plant dependent in this setup). Models 1 - 5 were therefore fitted to the data and model selection was performed. Model 2 was the best-supported model (Table 2 and Fig. 3). Although the fit (i.e., NLL) of Models 4 and 5 is slightly better, model selection with AIC shows that the data provide less support for these models: the minor improvement in model fit does not compensate for the addition of extra parameters into the model (Table 2). Model 2 allows each particle type to have its own probabilities of invasion (α) and systemic infection (β), but does not include host-plant-dependent infection probabilities or non-additive interactions between particles during infection.

Effects of the expression of genome segments on secondary infection

Given the large differences in systemic infection probabilities predicted by both models (Tables 1 and 2), we expected to observe qualitative differences in infection dynamics between the different plant types. To study infection dynamics, the area of primary infection foci at two time points was measured (Fig. 4a). If primary infection foci expand rapidly, then

365 the probability of systemic infection may be larger; the virus may then reach vascular tissue
366 before host responses limit its expansion (11, 22). There was a significant effect of plant
367 type on the area of primary infection foci (GLM: P = 0.001), and there were significant
368 differences in area between all plant types (P < 0.001 for all pairwise comparisons).
369 Moreover, there also appeared to be differences in the intensity of fluorescence, with lower
370 fluorescence in wild-type than in P2 and P12 plants (Fig. 4b-d). In all cases, the differences
371 are in line with expectations based on estimated probabilities of primary infection: P12 > P2 >
372 wild-type for foci area and fluorescence intensity.

373 Whether there was evidence for qualitative differences in AMV systemic infection in
374 the three different plants used was also considered. There appear to be fewer systemically
375 infected leaves in systemically infected P2 and wild-type plants than in P12 plants (Fig. 5).
376 To test if this effect was significant, the data from systemically infected plants at all doses
377 were pooled and then performed a χ^2 test for trend in proportions. A highly significant effect
378 of plant type was found (χ^2 = 13.476, 1 d.f., P < 0.001) overall. Pairwise comparisons
379 showed that there are not significant differences between wild-type and P2 plants (P =
380 0.377), whereas there are significantly more leaves infected in P12 plants than in wildtype or
381 P2 plants (P < 0.001 for both comparisons).

382

383 **Discussion**

384 The infection kinetics of AMV, a tripartite virus, was studied in wild-type tobacco plants and
385 transgenic plants expressing one (P2) or two (P12) AMV genome segments (15). A steep
386 dose response was found in wild-type plants, concordant with previous results for multipartite
387 viruses (5, 12). A rigorous analysis of the data with the classic infection model, which
388 assumes the three types of virus particles occur at the same frequency in the inoculum, was
389 therefore highly congruent with these historical results. For P2 plants similar results were
390 obtained, confirming that IAH model predictions are not supported for tripartite viruses, even

391 when the host plant expresses one genomic segment. On the other hand, for P12 plants the
392 dose response was shallower and IAH model predictions were supported. These
393 observations show that expression of 2 viral RNA segments in the host plant could modify
394 the infection kinetics of a tripartite virus to those of a monopartite virus.

395 Analysis of dose response with the classical infection model assumes that all three
396 types of virus particles occur at the same frequency. However, it was found that the different
397 particle types were not present at the same frequency. Specifically, the virus particle
398 containing RNA3 was present at a relatively low frequency. We have not encountered a
399 discussion of the frequency of different particle types in the literature on multipartite viruses.
400 Nevertheless, published primary data on AMV support the particle frequencies observed
401 here. The ultracentrifugation patterns (i.e., Schlieren peaks) obtained for two AMV
402 preparations show a lower peak for middle component than bottom component, whilst top
403 component is almost as abundant as bottom component (Fig. 1 on pg. 521 of reference
404 (29)). The frequency of RNA3 is so low that ´top component´ in ultracentrifugation studies
405 probably corresponds mainly to particles encapsulating RNA4. Electrophoresis of RNA
406 purified from AMV particles clearly shows that (i) RNAs 1 and 4 are the most abundant, (ii)
407 that levels of RNA2 are intermediate, and (iii) that RNA3 is scarce (Fig. 7 on pg. 97 of
408 reference (3)). This congruence in observed patterns suggests that the frequency of
409 particles estimated here might be a general pattern for AMV.

410 The different frequencies at which different virus particle types occur have
411 implications for the shape and position of the dose response. Given the scarcity of RNA3,
412 the dose response for wild-type plants would be predicted to be similar to that predicted by
413 the IAH model (Fig. 1e). The empirical dose response is, however, significantly steeper than
414 IAH model predictions (Fig. 2a). Data were therefore analyzed with a general infection
415 model, and model selection identified Model 2 as the best-supported model. This model
416 incorporates the empirically measured frequencies of particle types and allows each particle
417 type to have its own probability of invasion and systemic infection. Parameter estimates for

Model 2 suggest the probability of invasion is more than 2 orders of magnitude higher for AMV particles encapsidating RNA3, whereas probabilities of invasion are more or less similar for the other two particle types (Table 2). Note that this result does not depend solely on analysis of infection in P2 and P12 plants alone; it also follows logically form observing both a steep dose response in wild-type plants and different frequencies of the different particle types. Moreover, what makes this modeling result compelling is that the probabilities of invasion and systemic infection for different particle types also account for the position of the dose response curves in the different plant types. Fig. 1 shows that the shape and position of the dose response curve are both dependent on the invasion probability, and these results show that Model 2 can also account for both. It would not have been surprising if the expression of genome segments by the host plant would have affected the probability of invasion of other viral segment, but the model-selection results suggest no such effect occurs (i.e., Model 2 has more support than Model 5). Therefore, from the perspective of the theoretical framework developed here, the experimental system used (i.e., transgenic plants expressing viral RNA segments) responds exactly as expected. This rigorous and complete analysis therefore confirms results from the preliminary analysis using the classical model. However, it also shows that in reality infection kinetics are more complicated, as the inclusion of differences in particle frequencies illustrates that there are differences in the invasion probabilities of different particle types.

What mechanisms might account for these differences in invasion probabilities? Effective ´invasion´ of cells in the inoculated leaf may require fewer molecules of RNA3 than molecules of RNAs 1 and 2. We are not hereby suggesting a threshold, as such a model would behave differently than the infection models presented here. Rather, the invasion process can be seen as two steps: (i) physically breaching the cell and then (ii) being capable of supporting the infection process. In this framework, particles of each type have an independent probability of being successful at either step. This suggests two mechanistic explanations of the model. First, RNA3 is the shortest genome segment, and as a

consequence particles encapsidating RNA3 may be considerably more stable than those containing RNAs 1 and 2, or they may enter cells in the inoculated leaf more easily. In both cases, the probability of breaching a cell would be higher. Second, it may be that the probability that a RNA3 molecule that has breached the cell can support replication is higher than that for RNAs 1 and 2. In this case, RNAs 1 and 2 might be degraded more quickly intracellularly. The fact that RNAs 1 and 2 code all the genes required for replication (15) suggests that these segments must prime the cell for replication, but that once a cell is primed the probability that an RNA3 molecule can successfully start a productive infection is considerably higher. One might therefore expect qualitative differences in infection dynamics between the different the host plants. Indeed, primary infection foci expanded more rapidly in P2 and P12 plants, whereas systemic movement appears to be enhanced only in P12 plants. These observations again suggest that little RNA3 is required during infection.

A key question that remains enigmatic is why multipartite genomes have evolved, and what adaptive advantages multipartition confers. Four possible adaptive advantages conferred by genome segmentation alone – as opposed to multipartition – have been suggested. These advantages to segmentation alone may be relevant to this discussion because multipartition itself might be a pleiotropic effect of segmentation. I.e., given that most plant viruses are non-enveloped, segmentation of the genome might inevitably lead to the formation of multiple virus particles. First, at the usually high genomic mutation rate of RNA viruses (30), a small segment would have a greater chance of being replicated without errors than a larger one (31). Second, reassortment could allow for rapid recombination, reducing the effects of clonal interference between beneficial mutations occurring on different genome segments while also bolstering purifying selection against deleterious mutations (32), although in one case reassortment appears to be scarce in the field for a multipartite virus (33). Third, segmentation could allow for regulation of expression, because each segment can have its own regulatory sequence, a hypothesis that has good experimental support (34). Finally, segmentation can in principle allow for faster replication of viral

genome, through the accommodation of additional transcriptional units (35). In addition to the advantages conferred by genome segmentation alone, dividing the genome over multiple virus particles could confer the following three advantages. First, recent work suggests that the stability of particles will be improved by having shorter genome segments and smaller particles with a lower packaging density (36, 37), lending credence to the view that encapsidation imposes limits on the size of genome fragments. Second, it has been suggested that vectors may transmit smaller particles more efficiently (38), although this hypothesis has, to our knowledge, not been tested. Nonetheless, an increased chance for complementation would, theoretically, favor the evolution of a multipartite genome (39). Third, recent work suggests that the frequencies of different genome segments evolve to distinct levels, suggesting virus particle frequencies might have a regulatory role in gene expression (40).

On the other hand, irrespective of the advantages it might confer, the packaging of different genome segments in multiple types of particles will also have a cost. This cost arises because infection requires the entry of all genome segments into the same cell, during primary and systemic infection of the plant. If the total number of genomes that enter a cell during both processes is not large and if there are no mechanisms that physically link the different particle types during between-host and between-cell transmission, there will be an appreciable probability that not all types of genome segments will be represented. Assuming the same probability of cellular infection per genome segment of the complete (monopartite virus) or partial genome (multipartite virus), the same number of encapsidated copies of the complete virus genome will in principle lead to lower levels of host infection for a multipartite virus than for a monopartite virus (39). The results presented here, however, strongly suggest that infection probabilities of the different virus particles can be highly divergent. We speculate on a further reason why multipartite viruses might have evolved, and a mechanism that mitigates the cost of multipartition. If the probability that RNA3 can support infection (i.e., invade a cell) is higher than that for RNAs 1 and 2, then the virus could efficiently infect

even if there are less copies of this segment present. Evolution could then favor the down-regulation of RNA3 sequences by means of multipartition. Down-regulation of RNA3 would then allow for reallocation of cell resources to produce more particles encapsidating RNAs 1 and 2, the limiting factors at the start of infection. This higher production could then, in principle, boost overall levels of infection and therefore be adaptive. More evidences will be necessary to show this hypothesis has merit, although it is compatible with other hypotheses for why multipartite viruses have evolved.

Acknowledgements:

The authors thank María D. Comin, Lorena Corachán, Francisca de la Iglesia, and Paula Agudo for excellent technical support.

JASN was supported by grant BIO2011-25018, MPZ by a ´Juan de la Cierva´ postdoctoral contract (JCI-2011-10379) and SFE by grant BFU2012-30805, all from the Spanish Secretaría de Estado de Investigación, Desarrollo e Innovación.

References

1. **Nelson MI, Viboud C, Simonsen L, Bennett RT, Griesemer SB, George KS, Taylor J, Spiro DJ, Sengamalay NA, Ghedin E, Taubenberger JK, Holmes EC.** 2008. Multiple reassortment events in the evolutionary history of H1N1 *Influenza A virus* since 1918. PLoS Pathog. **4**:e1000012.
2. **Rambaut A, Pybus OG, Nelson MI, Viboud C, Taubenberger JK, Holmes EC.** 2008. The genomic and epidemiological dynamics of human *Influenza A virus*. Nature **453:**615-619.
3. **Jaspars EM.** 1974. Plant viruses with a multipartite genome. Adv. Virus Res. **19:**37-149.
4. **Gronenborn B.** 2004. Nanoviruses: genome organisation and protein function. Vet. Microbiol. **98:**103-109.
5. **Fulton RW.** 1962. Effect of dilution on *Necrotic ringspot virus* infectivity and enhancement of infectivity by noninfective virus. Virology **18:**477-485.
6. **Bald JG.** 1937. The use of numbers of infections for comparing the concentration of plant virus suspensions I. Dilution experiments with purified suspensions. Ann. Appl. Biol. **24:**33-55.
7. **Zwart MP, Daròs JA, Elena SF.** 2011. One is enough: *In vivo* effective population size is dose-dependent for a plant RNA virus. PLoS Pathog. **7**:e1002122.
8. **Zwart MP, Hemerik L, Cory JS, de Visser JAGM, Bianchi FJJA, van Oers MM, Vlak JM, Hoekstra RF, van der Werf W.** 2009. An experimental test of the

independent action hypothesis in virus-insect pathosystems. Proc. R. Soc. B **276:**2233-2242.

9. **Furumoto WA, Mickey R.** 1967. A mathematical model for infectivity-dilution curve of *Tobacco mosaic virus* - experimental tests. Virology **32:**224-233.
10. **Lafforgue G, Tromas N, Elena SF, Zwart MP.** 2012. Dynamics of the establishment of systemic potyvirus infection: Independent yet cumulative action of primary infection sites. J. Virol. **86:**12912-12922.
11. **Zwart MP, Daròs JA, Elena SF.** 2012. Effects of potyvirus effective population size in inoculated leaves on viral accumulation and the onset of symptoms. J. Virol. **86:**9737-9747.
12. **Price WC, Spencer EL.** 1943. Accuracy of the local lesion method for measuring virus activity. II. *Tobacco necrosis*, *Alfalfa mosaic*, and *Tobacco ringspot viruses*. Am. J. Bot. **30:**340-346.
13. **Bald JG.** 1950. Measurement of concentration of plant virus suspensions, p. 17-29. In M. Delbrück (ed.), Viruses 1950. California Institute of Technology, Pasadena, California, USA.
14. **Lauffer MA, Price WC.** 1945. Infection by viruses. Arch. Biochem. **8:**449-468.
15. **Taschner PEM, Vanderkuyl AC, Neeleman L, Bol JF.** 1991. Replication of an incomplete *Alfalfa mosaic virus* genome in plants transformed with viral replicase genes. Virology **181:**445-450.
16. **Sánchez-Navarro JA, Bol JF.** 2001. Role of the *Alfalfa mosaic virus* movement protein and coat protein in virus transport. Mol. Plant Microbe Interact. **14**: 1051-1062.
17. **Tenllado F, Bol JF.** 2000. Genetic dissection of the multiple functions of *Alfalfa mosaic virus* coat protein in viral RNA replication, encapsidation, and movement. Virology **268**: 29-40.
18. **Van der Vossen EA, Neeleman L, Bol JF.** 1994. Early and late functions of *Alfalfa mosaic virus* coat protein can be mutated separately. Virology **202**: 891-903.
19. **Vloten DL, Jaspars EM.** 1972. The uncoating of *Alfalfa mosaic virus* by its own RNA. Virology **48**:699-708.
20. **Regoes RR, Hottinger JW, Sygnarski L, Ebert D.** 2003. The infection rate of *Daphnia magna* by *Pasteuria ramosa* conforms with the mass-action principle. Epidemiol. Infect. **131**:957-966.
21. **Van der Werf W, Hemerik L, Vlak JM, Zwart MP.** 2011. Heterogeneous host susceptibility enhances prevalence of mixed-genotype micro-parasite infections. PLoS Comput. Biol. **7**:e1002097.
22. **Fajardo TV, Peiró A, Pallás V, Sánchez-Navarro, J.** 2013. Systemic transport of *Alfalfa mosaic virus* can be mediated by the movement proteins of several viruses assigned to five genera of the 30K family. J. Gen. Virol. **94**:677-681.
23. **Sánchez-Navarro JA, Cañizares MC, Cano EA, Pallás V.** 1999. Simultaneous detection of five carnation viruses by non-isotopic molecular hybridization. J. Virol. Meth. **82**:167-175.
24. **Pallás V, Mas P., Sánchez-Navarro JA.** 1998. Detection of plant RNA viruses by nonisotopic dot-blot hybridization. Methods Mol. Biol. **81**:461-468.
25. **Sánchez-Navarro J, Miglino R, Ragozzino A, Bol JF.** 2001. Engineering of *Alfalfa mosaic virus* RNA3 into an expression vector. Arch. Virol. **146**:923-939.
26. **Neeleman L, Bol JF.** 1999. Cis-acting functions of *Alfalfa mosaic virus* proteins involved in replication and encapsidation of viral RNA. Virology **254**:324-333.
27. **Schneider CA, Rasband WS, Eliceiri KW.** 2012. NIH Image to ImageJ: 25 years of image analysis. Nat. Meth. **9:**671-675.
28. **Nassuth A, Bol JF.** 1983. Altered balance of the synthesis of plus strand and minus strand RNAs induced by RNA1 and RNA2 of *Alfalfa mosaic virus* in the absence of RNA3. Virology **124:**75-85.

29. **Bancroft JB, Kaesberg P.** 1960. Macromolecular particles associated with *Alfalfa mosaic* virus. Biochim. Biophys. Acta **39:**519-527.
30. **Sanjuán R, Nebot MR, Chirico, N, Mansky LM, Belshaw, R.** 2010. Viral mutation rates. J. Virol. **84**: 9733-974.
31. **Pressing J, Reanney DC.** 1984. Divided genomes and intrinsic noise. J. Mol. Evol. **20**:135-146.
32. **Chao L.** 1991. Levels of selection, evolution of sex in RNA viruses, and the origin of life. J. Theor. Biol. **153:**229-246.
33. **Fraile A, Alonso-Prados JL, Aranda MA, Bernal JJ, Malpica JM, García-Arenal F.** 1997. Genetic exchange by recombination or reassortment is infrequent in natural populations of a tripartite RNA plant virus. J. Virol. **71:**934-940.
34. **Sullivan ML, Ahlquist P.** 1997. Cis-acting signals in bromovirus RNA replication and gene expression: Networking with viral proteins and host factors. Sem. Virol. **8:**221-230.
35. **Takeda M, Nakatsu Y, Ohno S, Seki F, Tahara M, Hashiguchi T, Yanagi Y.** 2006. Generation of measles virus with a segmented RNA genome. J. Virol. **80**:4242-4248.
36. **Iranzo J, Manrubia SC.** 2012. Evolutionary dynamics of genome segmentation in multipartite viruses. Proc. R. Soc. B **279:**3812-3819.
37. **Ojosnegros S, García-Arriaza J, Escarmis C, Manrubia SC, Perales C, Arias A, Mateu MG, Domingo E.** 2011. Viral genome segmentation can result from a trade-off between genetic content and particle stability. PLoS Genet. **7**:e1001344.
38. **Goldbach RW.** 1986. Molecular evolution of plant RNA viruses. Annu. Rev. Phytopathol. **24:**289-310.
39. **Nee S.** 1987. The evolution of multicompartmental genomes in viruses. J. Mol. Evol. **25**:277-281.
40. **Sicard A, Yvon M, Timchenko T, Gronenborn B, Michalakis Y, Gutiérrez S, Blanc S.** Nat. Commun., In press.

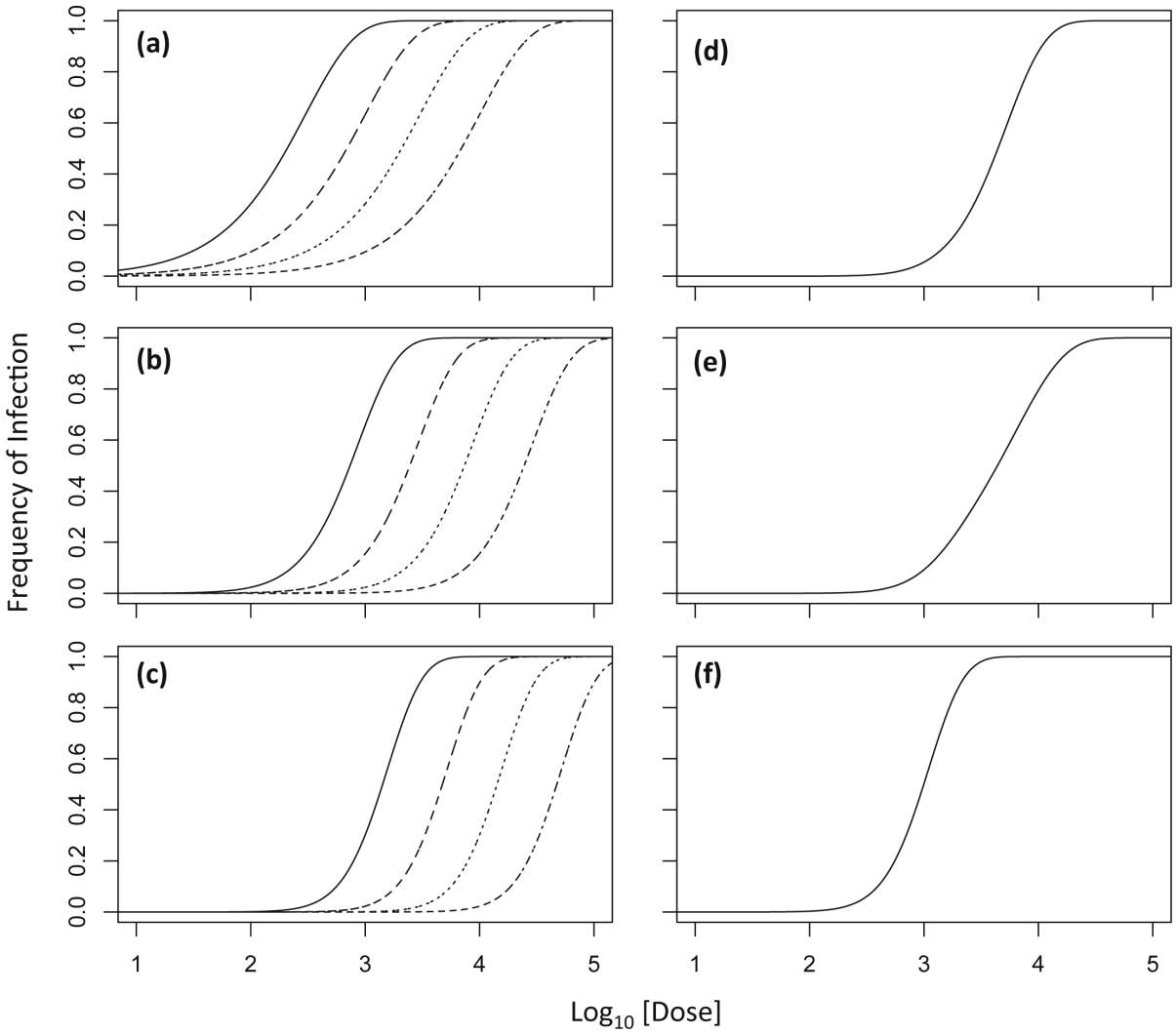

Figure 1: Infection model predictions

For all panels, the $\log_{10}$-transformed dose is on the abscissae (where dose is the sum of the doses for each type of virus particle), and the infection frequency is on the ordinate. In panel a, predictions of the infection model for virus with 1 genome segment (k = 1; IAH) are shown, with infection probabilities decreasing from 3.3×10^{-3}, 1×10^{-3}, 3.3×10^{-4} and 1×10^{-4}, for the curves from left to right (the grain of the dotted line becomes finer as infection probability decreases). Note that changing the infection probability shifts the curve, but does not alter its shape. Panels b and c show model predictions for a virus with two (k = 2) and three (k = 3) genome segments at the equal frequencies for different particle types, respectively, and the same infection probabilities. Note that whilst genome segment number alters the shape

628 of the curve, changing infection probability only changes its shape. Panel d shows model
629 predictions for a tripartite virus in which each segment has an infection probability of 3.3×10^{-3}, but one segment has a ten-fold higher frequency than the other two. The shape of the
631 dose response is then similar to that of a bipartite virus. Panel e shows model predictions for
632 a tripartite virus in which each segment has an infection probability of 3.3×10^{-3}, but one
633 segment has a ten-fold lower frequency than the other two. The dose response is then
634 similar to that of a monopartite virus. In panel f, the frequency of the different particle types
635 is the same, but the probability of infection for the rare segment is 3.3×10^{-2}. The dose
636 response is then as steep as possible for a tripartite virus in the absence of non-additive
637 interactions (k is equal to the actual number of genome segments, or $\omega = 1$), even though
638 particle frequencies are different.
639

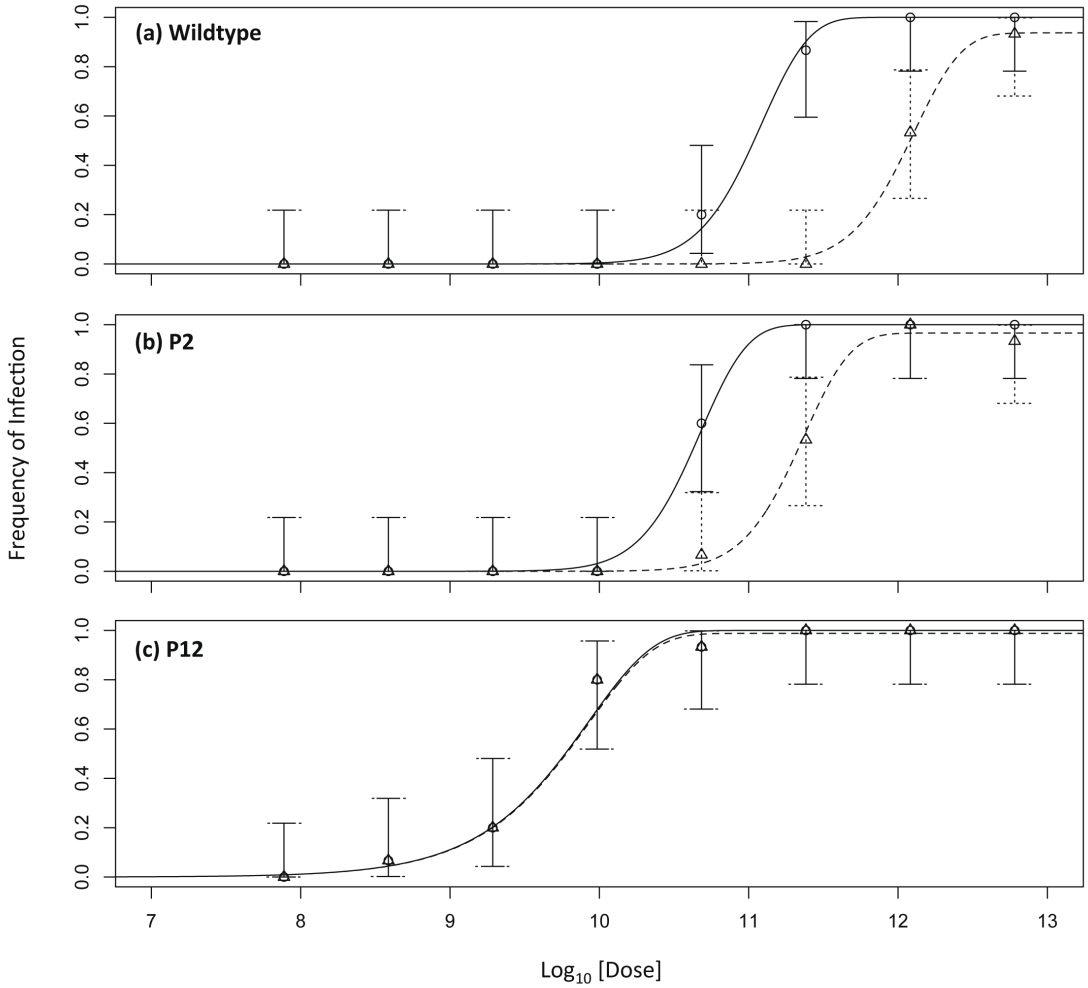

640

641 **Figure 2: Data and model predictions for different plant types**

642 For all panels, the $\log_{10}$-transformed total dose of particles is on the abscissa and the
643 frequency of infection is on the ordinate. Dose is the sum of the doses for all three particle
644 types. Solid lines represent the predicted dose response for infection of the inoculated of the
645 best-supported model; DA for wild-type and P2 plants, IAH for P12 plants. The dotted lines
646 represent the model prediction of dose response for systemic infection. Circles represent the
647 data for infection of the inoculated leaf, and triangles represent the systemic infection data.
648 Errors bars indicate the 95% confidence interval. Note the steeper dose responses for wild-
649 type and P2 plants, and the decrease between the dose response for the inoculated leaf and
650 systemic tissue, from wild-type to P2 to P12, at which point the two curves practically
651 coincide. For parameter estimates see Table 1.

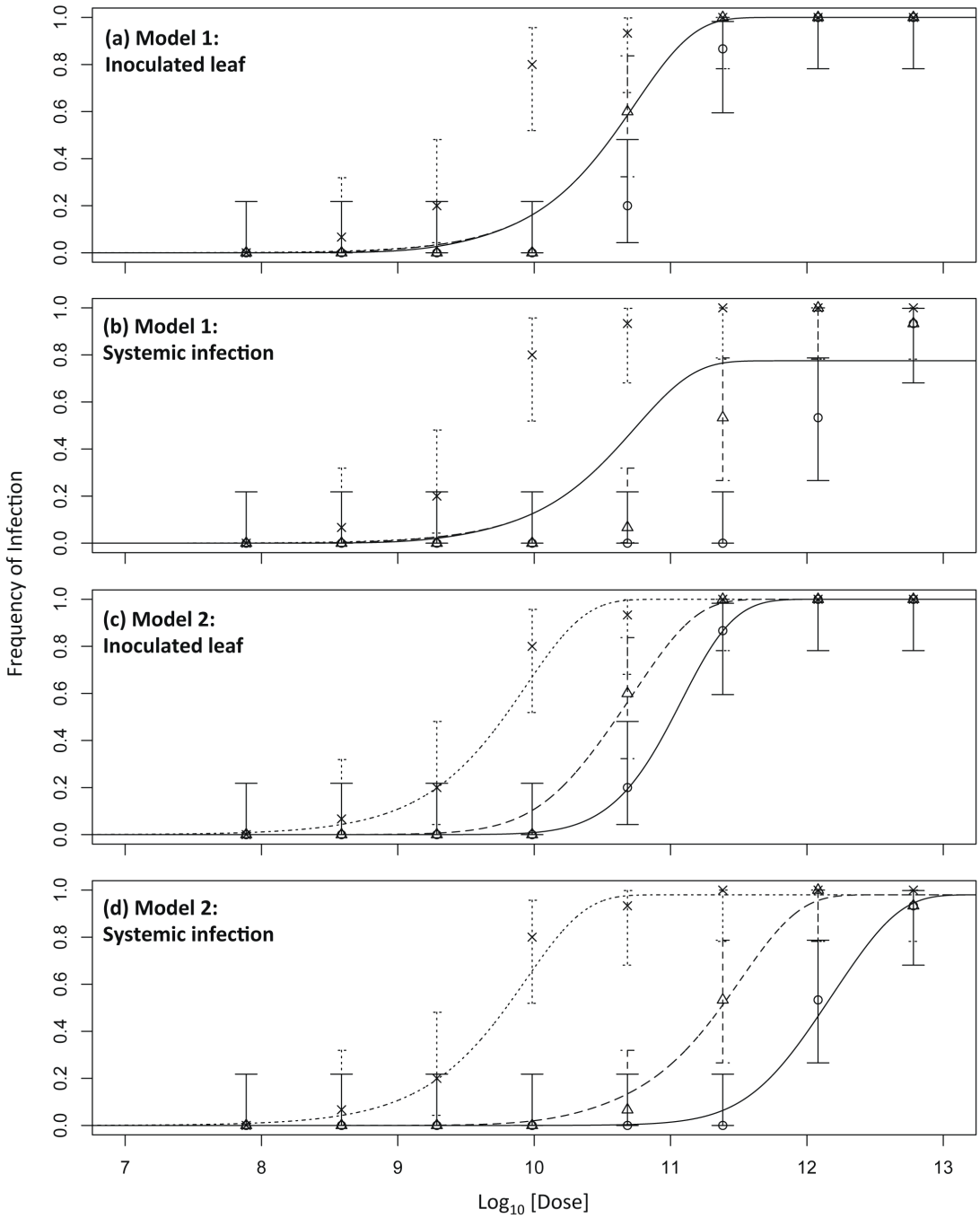

652

653 **Figure 3: Effects of genome-segment number on dose response**

654 For all panels, the $\log_{10}$-transformed dose is on the abscissae and the frequency of infection
655 is on the ordinate. Dose is the sum of the doses for all particle types. Solid lines represent
656 the predicted dose response for wild-type plants, coarse dotted lines for P2 plants, and fine
657 dotted lines for P12 plants. Circles are the data for wildtype plants, triangles P2 plants and

crosses P12 plants, with errors bars indicating the 95% confidence interval. Panel a shows the results for Model 1 fitted to the inoculated leaf data, panel b the results of Model 1 for systemic infection, panel c the results of Model 2 for the inoculated leaf, and panel d the results of Model 2 for systemic infection. Both models include the empirically determined frequency of different particle types. Model 1 fits the data poorly, because the invasion probability for all particle types is the same. The most abundant particle type (RNA1) then in fact determines the infection kinetics, resulting in a response that is indifferent to the plant type. Model 2 allows each particle type to have a different infection probability, even thought these infection probabilities do not depend on the plant type (i.e., Model 5), and fits the data much better. Model 3 (not shown) fit the data poorly. Models 4 and 5 (not shown) fit the data slightly better than Model 2, but model selection indicated that the improvements in fit did not justify the additional free parameters added.

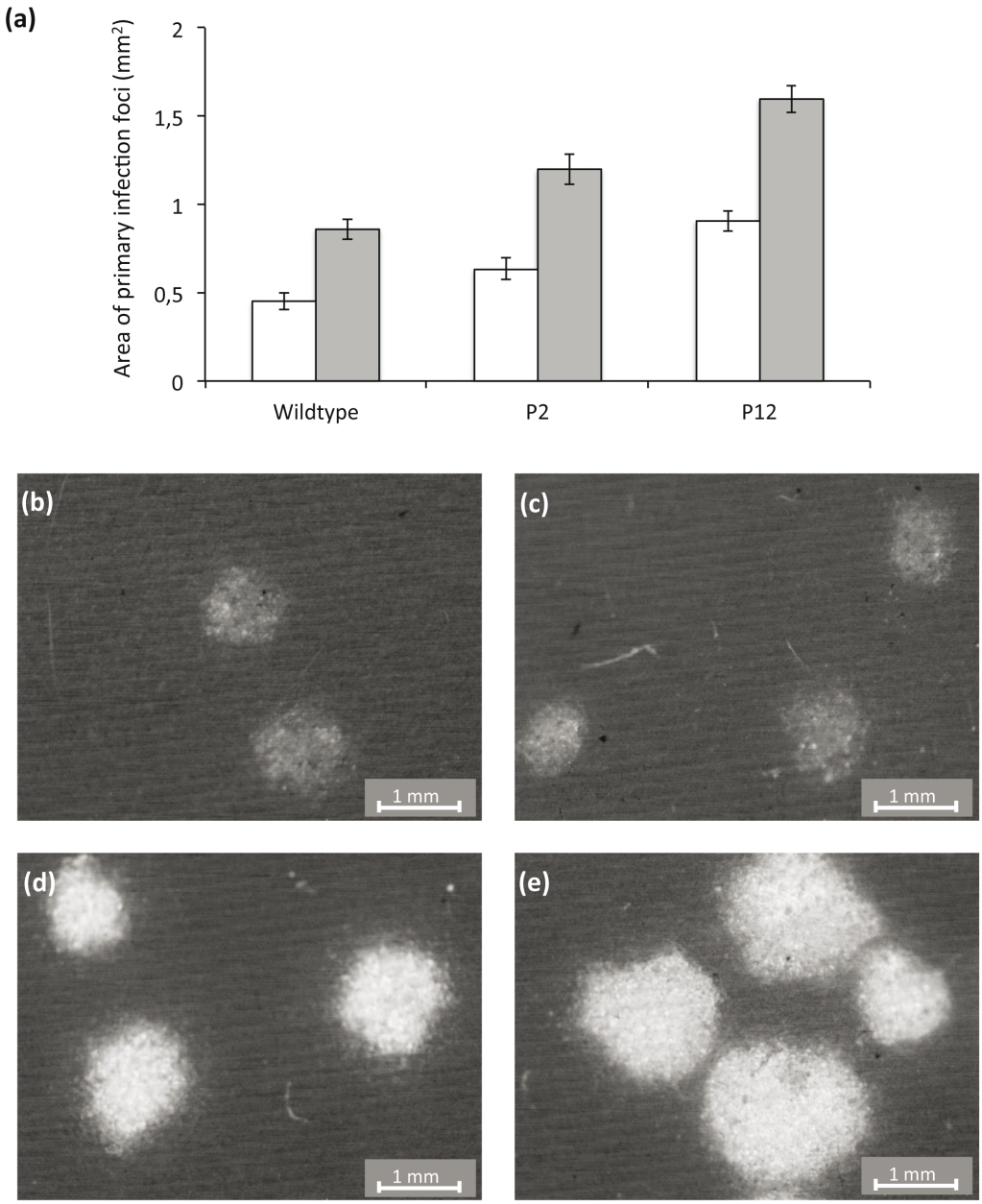

671

672 **Figure 4: Effects of plant type on virus expansion in primary infection foci**

673 Panel a gives the area (mm^2) of primary infection foci at 2 (white bars) and 3 (gray bars) dpi,
674 for the three plant types used. The error bars represent the 95% CI. Primary infection foci at
675 3 dpi are shown for the wild-type (panels b and c), P2 (panel d) and P12 (panel e) plants.
676 Besides the differences in size, the foci for the P2 and P12 plants have a higher intensity of
677 fluorescence, suggesting that there are higher levels of infection.

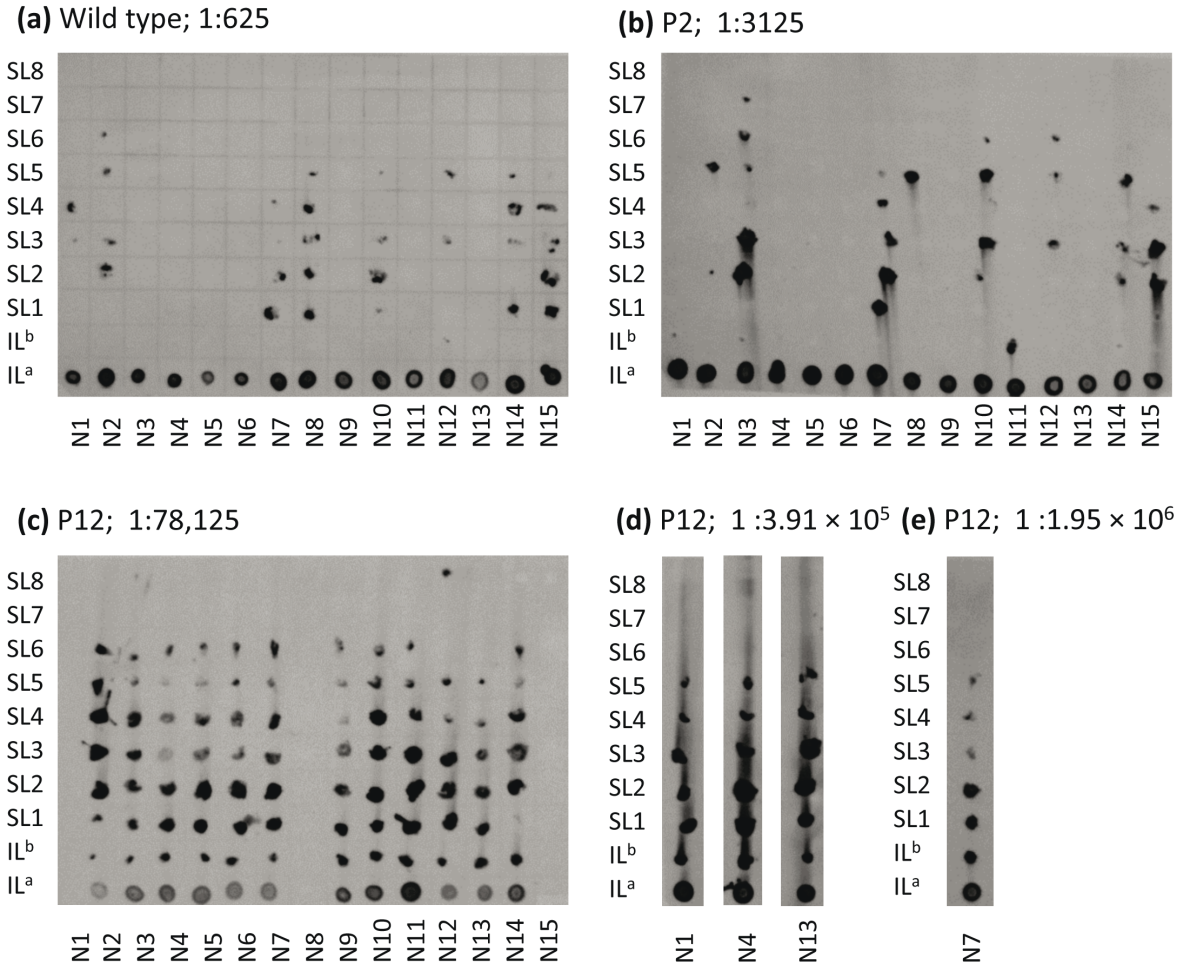

Figure 5: Effects of plant type on systemic infection

All leaves from inoculated tobacco plants were sampled, and tissue-printing analysis was performed. To compare the effects of plant type on systemic infection, the lowest dose for which the majority of inoculated plants were infected was considered, even though this dose was smaller for P12 than for P2 than for wild-type plants. In the above figure, the blots are given for each plant type, with the dilution specified by the ratio right of the plant type. N-label columns indicate the plant replicate, and rows indicate the leaf. IL^a is the inoculated leaf (ground whole leaf), IL^b is the inoculated leaf stem, SL are the numbered stems of systemic leaves, with SL1 being the leaf above the inoculated leaf. For P12 plants the data for even higher dilutions are also given, to show that at all doses all leaves remain infected (panels d and e).

690 **Table 1: Model fitting and selection results for testing the IAH and DA models [a]**

Plant	Model	Parameter estimates	NLL	AIC	ΔAIC	AW
Wild-type	IAH	α = 6.46 [4.17-10.23] × 10^{-12} β = 7.08 [4.07-16.22] × 10^{-2} ψ = 1 [0.830-1]	9.273	24.545	4.557	0.093
	DA	α = 1.35 [0.89-2.57] × 10^{-12} β = 9.54 [4.90-16.98] × 10^{-2} k = 2.635 [1.912-3.426] ψ = 0.937 [0.806-1]	5.994	19.989	-	0.907
P2	IAH	α = 1.55 [1.07-2.45] × 10^{-11} β = 0.204 [0.079-0.372] ψ = 0.965 [0.893-1]	10.407	26.814	5.609	0.057
	DA	α = 3.55 [2.40-5.62] × 10^{-11} β = 0.204 [0.060-0.363] k = 2.801 [2.067-3.630] ψ = 0.996 [0.895-1]	6.603	21.206	-	0.943
P12	IAH	α = 1.20 [0.25-2.04] × 10^{-10} β = 1 [*] ψ = 0.987 [0.922-1]	14.226	34.452	-	0.600
	DA	α = 7.59 [1.91-25.70] × 10^{-11} β = 1 [0.977-1] k = 0.731 [0.521-1.380] ψ = 1 [0.926-1]	13.633	35.265	0.814	0.400

691

692 [a] Data for each plant type was analyzed separately here, to determine whether the IAH
693 (independent action hypothesis) or DA (dependent action) model is best supported by the
694 data. For the wild-type and P2 plants, we expect to reject this model as three and two
695 particles types, respectively, are required for infection. For the P12 plant, we expect the
696 hypothesis to be supported because only one particle type is required for infection, as the
697 other two are supplied *in trans* by the plant. Model parameter estimates and their 95%
698 confidence intervals are given. NLL is the negative log likelihood, a measure of model fit.
699 AIC is the Akaike Information Criterion, ΔAIC is the different between a given model and the
700 best fitting model, and AW is the Akaike Weight, a measure of the relative support for the
701 model. Note that comparison between models is always for a given plant type. * indicates
702 that the lower and upper 95% CI limits coincide with the estimate parameter value.

703

Table 2: Model fitting and selection results for Models 1-5[a]

Model	Parameter estimates	NLL	AIC	ΔAIC	AW
1	α = 2.95 [2.19-4.17] × 10^{-9} β = 1 [0.209-1] ψ = 0.775 [0.775-0.948]	152.742	311.483	237.805	0
2	α_1 = 2.34 [0.11-8.51] × 10^{-11} α_2 = 3.24 [0.11-8.91] × 10^{-11} α_3 = 1.86 [0.10-9.77] × 10^{-8} β_1 = 0.182 [0.032-0.295] β_2 = 6.17 [3.16-100] × 10^{-2} β_3 = 1 [0.324-1] ψ = 0.981 [0.901-0.998]	29.839	73.678	-	0.667
3	α = 2.82 [2.29-28.84] × 10^{-9} β = 0.525 [0.209-0.776] ω = 0.949 [0.949-1.047] ψ = 0.845 [0.777-0.953]	150.903	309.806	236.128	0
4	α_1 = 2.45 [1.07-8.91] × 10^{-11} α_2 = 3.24 [1.07-9.55] × 10^{-11} α_3 = 2.00 [1.12-9.12] × 10^{-8} β_1 = 0.182 [0.34-0.302] β_2 = 6.46 [3.47-100] × 10^{-2} β_3 = 1 [0.123-1] ω = 1.047 [0.953-1.048] ψ = 0.980 [0.902-0.998]	29.768	75.768	1.858	0.264
5	$\alpha_{1,WT}$ = 2.51 [0.81-11.48] × 10^{-11} $\alpha_{1,P2}$ = 4.57 [2.23-16.57] × 10^{-11} α_2 = 1.51 [0.19-2.88] × 10^{-10} $\alpha_{3,WT}$ = 1.41 [0.79-14.79] × 10^{-9} $\alpha_{3,P2}$ = 3.72 [0.45-6.31] × 10^{-9} $\alpha_{3,P12}$ = 1.78 [0.36-3.63] × 10^{-8} β_1 = 0.102 [0.043-0.234] β_2 = 1.45 [0.81-16.60] × 10^{-2} β_3 = 1 [0.295-1] ω = 0.976 [0.952-1.048] ψ = 0.980 [0.943-1]	28.105	78.210	4.532	0.069

[a] Data for all three plant types was analyzed jointly here, to determine whether the general infection model, incorporating differences in the frequencies of different types, could adequately explain the dose-response data. Model parameter estimates and their 95% confidence intervals are given. NLL is the negative log likelihood, a measure of model fit. AIC is the Akaike Information Criterion, ΔAIC is the different between a given model and the best fitting model, and AW is the Akaike Weight, a measure of the relative support for the model.